pH-dependent modulation of voltage gating in connexin45 homotypic and connexin45/connexin43 heterotypic gap junctions

Nicolas Palacios-Prado[a], Stephen W. Briggs[a], Vytenis A. Skeberdis[a], Mindaugas Pranevicius[b], Michael V. L. Bennett[a,1], and Feliksas F. Bukauskas[a,1]

[a]Dominick P. Purpura Department of Neuroscience and [b]Department of Anesthesiology, Albert Einstein College of Medicine, Bronx, NY 10461

Contributed by Michael V. L. Bennett, April 12, 2010 (sent for review January 15, 2010)

Intracellular pH (pH_i) can change during physiological and pathological conditions causing significant changes of electrical and metabolic cell–cell communication through gap junction (GJ) channels. In HeLa cells expressing wild-type connexin45 (Cx45) as well as Cx45 and Cx43 tagged with EGFP, we examined how pH_i affects junctional conductance (g_j) and g_j dependence on transjunctional voltage (V_j). To characterize V_j gating, we fit the g_j–V_j relation using a stochastic four-state model containing one V_j-sensitive gate in each apposed hemichannel (aHC); aHC open probability was a Boltzmann function of the fraction of V_j across it. Using the model, we estimated gating parameters characterizing sensitivity to V_j and number of functional channels. In homotypic Cx45 and heterotypic Cx45/Cx43-EGFP GJs, pH_i changes from 7.2 to ∼8.0 shifted g_j–V_j dependence of Cx45 aHCs along the V_j axis resulting in increased probability of GJ channels being in the fully open state without change in the slope of g_j dependence on V_j. In contrast, acidification shifted g_j–V_j dependence in the opposite direction, reducing open probability; acidification also reduced the number of functional channels. Correlation between the number of channels in Cx45-EGFP GJs and maximal g_j achieved under alkaline conditions showed that only ∼4% of channels were functional. The acid dissociation constant (pK_a) of g_j–pH_i dependence of Cx45/Cx45 GJs was ∼7. The pK_a of heterotypic Cx45/Cx43-EGFP GJs was lower, ∼6.7, between the pK_as of Cx45 and Cx43-EGFP (∼6.5) homotypic GJs. In summary, pH_i significantly modulates junctional conductance of Cx45 by affecting both V_j gating and number of functional channels.

cell-cell coupling | pH-dependent gating | EGFP | hemichannel | connexon

Changes in intracellular pH (pH_i) take place under different physiological and pathological conditions, and H^+ ions have a broad effect on cell function including cell–cell electrical and metabolic communication mediated by gap junctions (GJs) and paracrine signaling through nonjunctional/unapposed hemichannels (1–4). Modest pH_i changes have been observed under normal physiological conditions [e.g., changes of neuronal activity or the resting potential (5, 6)], and greater changes occur under pathological conditions such as hypoxia, ischemia, or epilepsy (4, 7, 8).

During the last decade, significant progress has been made toward understanding the molecular mechanisms of pH-dependent modulation of GJs and hemichannels (2, 9–12). Several domains in the cytoplasmic loop and C terminus of connexin43 (Cx43) appear to be involved in pH-dependent gating (2, 9, 11, 12). Furthermore, pH-dependent interaction of connexins with other cytoplasmic proteins may be important in the remodeling of connexins and in protection from lesion spread after local ischemic injury (13, 14).

GJs provide channels with an inner diameter of ∼1.4 nm between the interiors of the coupled cells. This link allows the spread of electrical potential and small metabolites. Each GJ channel is composed of two apposed hemichannels (aHCs) or connexons, each with six connexin subunits. aHCs can be homomeric (all subunits of the same connexin isoform) or heteromeric (containing more than one connexin isoform). GJ channels can be homotypic or heterotypic, i.e., formed by the same or different aHCs. Different connexin compositions can lead to differences in single-channel conductance, permselectivity, and/or asymmetric voltage gating (15, 16).

Each aHC has two mechanisms of gating in response to transjunctional voltage (V_j), the fast gate and the slow (or loop) gate (17) (Figs. S1 and S2). In addition, GJ channels can be gated by intracellular H^+, Ca^{2+}, posttranslational modifications, and a variety of chemical agents (18). The mechanisms by which these factors exert their effect on GJs remains unclear, although H^+ and Ca^{2+} ions may both act through the slow V_j gate (11).

Here, we characterize pH_i-dependent modulation of Cx45 GJs in HeLa cells expressing wild-type Cx45 or Cx45 tagged on its C terminus with green fluorescent protein (Cx45-EGFP). We also study heterotypic Cx45/Cx43-EGFP junctions to enable more accurate analysis of Cx45 aHCs. We found that much of the pH_i-dependent change in junctional conductance (g_j) could be explained by modulation of the voltage-gating properties. In addition, the number of functional channels (N_F), i.e., those that can be gated by V_j, increased modestly during alkalinization to approach a maximum but decreased markedly during acidification. From estimates of the total number of GJ channels, g_j as a function of pH_i, and single-channel conductance, we calculate that at alkaline pH_i only ∼4% of the GJ channels in junctional plaques (JPs) are functional; the remaining 96% appear to be permanently closed (Fig. S2). Thus, pH_i affects g_j by shifting the g_j–V_j relation of the aHCs along the V_j axis as well as by altering the number of channels that can open.

Results

pH_i-Dependent Modulation of the Conductance of Cx45 GJs. Junctional conductance (g_j) between HeLa cells expressing Cx45 or Cx45-EGFP was measured by dual voltage-clamp and application of repeated V_j ramps, 600 ms in duration, from +10 to −10 mV (Fig. 1*A*, *Inset*). In the Cx45 cell pairs studied, g_j under control conditions (pH_i = 7.2) varied between 6 and 47 nS (n = 29). In HeLaCx45-EGFP cell pairs, g_j under control conditions varied between 1.4 and 76 nS (n = 18), and, in general, g_j was higher in cell pairs with larger JPs visualized by their EGFP fluorescence.

To examine g_j as a function of pH_i, we used CO_2 or ammonium chloride (NH_4Cl) to reduce or increase pH_i, respectively. Cells

Author contributions: N.P.-P., V.A.S., M.P., M.V.L.B., and F.F.B. designed research; N.P.-P., S.W.B., V.A.S., and F.F.B. performed research; M.P. contributed new reagents/analytic tools; N.P.-P., S.W.B., V.A.S., M.P., M.V.L.B., and F.F.B. analyzed data; and N.P.-P., M.V.L.B., and F.F.B. wrote the paper.

The authors declare no conflict of interest.

[1]To whom correspondence may be addressed. E-mail: feliksas.bukauskas@einstein.yu.edu or michael.bennett@einstein.yu.edu.

This article contains supporting information online at www.pnas.org/lookup/suppl/doi:10.1073/pnas.1004552107/-/DCSupplemental.

PHYSIOLOGY

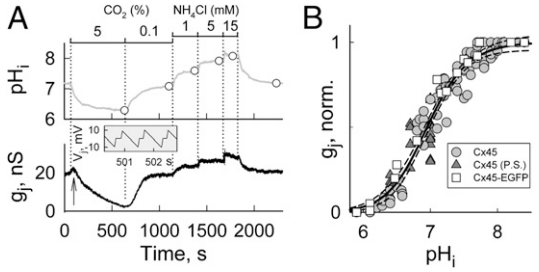

Fig. 1. pH_i-dependent modulation of g_j in homotypic Cx45 GJs. (*A*) Junctional conductance (g_j) measurements in a HeLaCx45 cell pair at different pH_is modulated by exposure to CO_2 and NH_4Cl. Repeated V_j ramps of ±10 mV in amplitude and 600 ms in duration (*Inset*) were used to measure g_j. (*B*) Normalized g_j–pH_i relations of GJs formed of Cx45 (circles) and of Cx45-EGFP (squares) with BCECF in the pipette to determine pH_i; these relations are superimposable. Triangles show g_j–pH_i dependence for experiments in which the pipette solution was buffered at different pHs and BCECF was omitted; pH_o remained constant (7.4); g_j was normalized to the maximum value at alkaline pH_i. Data for Cx45 (circles) were fit by the Hill equation (solid black curve); $pK_a = 6.96 \pm 0.03$; Hill coefficient **n** = 1.43 (n = 12). Thinner dashed lines show 95% confidence interval (CI).

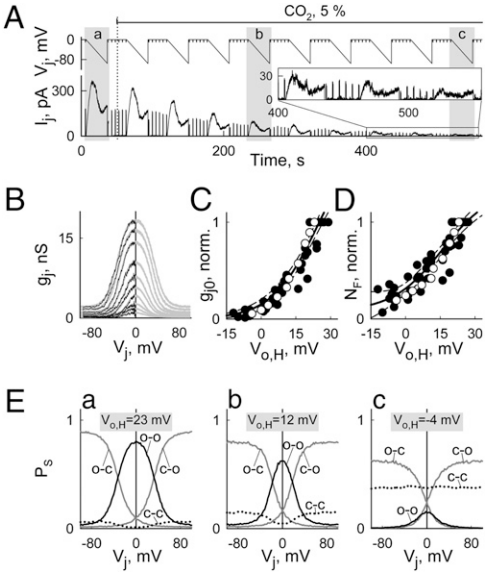

Fig. 2. V_j gating during acidification of homotypic Cx45 GJs. (*A*) I_j measured in a HeLa Cx45 cell pair in response to repeated V_j ramps (31 s duration) from 0 to −100 mV before and during exposure to 5% CO_2. V_j steps of −10 mV were used to measure g_j between V_j ramps. (*B*) Experimental g_j–V_j plots (in black) were fit by the S4SM (in gray) assuming that V_j gating was symmetric around V_j = 0. (*C*) Relation between g_j at V_j = 0 (g_{jo}; normalized to control/initial conditions) and $V_{o,H}$ (black and white circles). (*D*) Relation between N_F normalized to control/initial conditions and $V_{o,H}$ (black and white circles). Solid lines in *C* and *D* are curves fit from combined data in Fig. 2 and Fig. 3, obtained using a sigmoidal equation, $y = a/(1+e^{-(x-xo)/b})$ (n = 12). Dashed lines show 95% CI. White circles are from the experiment shown in *A*. (*Ea–c*) Probabilities of channels to dwell in O-O, C-O, O-C, and C-C states (P_S) depending on V_j and calculated for the three I_j records obtained during V_j ramps *a–c* marked with gray rectangles in *A*; calculated values of $V_{o,H}$ are indicated.

were exposed to modified Krebs-Ringer (MKR) solutions bubbled with CO_2 or with added NH_4Cl, and the unesterified form of the ratiometric fluorescent probe, 2,7-bis(2-carboxyethyl)-5(6)-carboxyfluorescein (BCECF), was dialyzed into the cells from the recording pipettes to measure pH_i (Fig. 1*A*) (19). Application of MKR solution bubbled with 5% CO_2 decreased pH_i to ∼6.3, resulting in almost complete uncoupling. CO_2 decreased extracellular pH (pH_o) as well, but g_j has been shown to be insensitive to external acidification (20). The small increase in g_j (arrow in Fig. 1*A*; also see Fig. 4*B*) as pH_i starts to decrease has been described (21). Application of 15 mM NH_4Cl increased pH_i from 7.2 ± 0.1 to 8.1 ± 0.2 (n = 18) and increased g_j on average to 1.8 times its value at pH_i = 7.2. Fitting the Hill equation to the g_j–pH_i relation for Cx45 (circles in Fig. 1*B*) yielded an acid dissociation constant (pK_a) equal 6.96 ± 0.03 and Hill coefficient **n** = 1.43 (n = 12). Values for Cx45-EGFP (squares in Fig. 1*B*) were not significantly different (pK_a = 6.90 ± 0.04 and Hill coefficient **n** = 1.45, n = 4). To test whether BCECF itself could affect our measurements, we used pipette solutions without BCECF and buffered to different pHs. After opening of the patches, g_j was measured after reaching a steady state. Then the cells were exposed to MKR solution containing a high concentration of NH_4Cl (20 mM) at pH_o ∼8, and the g_j–pH_i relation was normalized to the maximum g_j. The observed g_j–pH_i dependence (triangles in Fig. 1*B*) overlapped the g_j–pH_i relation determined using the BCECF probe, a convergence validating both approaches.

pH-Dependent Modulation of V_j Gating in Cx45 GJ Channels. We examined g_j–V_j dependence of homotypic Cx45 GJs during acidification (Fig. 2) and alkalinization (Fig. 3). Because homotypic junctions typically demonstrate symmetric g_j–V_j dependence, we measured junctional current (I_j) only in response to 31-s V_j ramps of negative polarity, from 0 to −110 mV (Figs. 2*A* and 3*A*). The experimental g_j–V_j relations calculated from I_j and V_j records are hemibell shaped with g_j maximal at V_j = 0 and markedly lower at more negative V_js (Figs. 2*B* and 3*B*, black curves). During acidification, g_j was reduced (Fig. 2 *A* and *B*); during alkalinization, g_j was increased (Fig. 3 *A* and *B*). To analyze V_j-gating properties, we fitted experimental g_j–V_j plots with a stochastic four-state model (S4SM) (Fig. S1) (22). The S4SM assumes that the voltage across each aHC in the junction depends on the conductance of the aHC in series ("contingent gating") (23) and allows us to define parameters characterizing V_j gating according to a Boltzmann relation, namely $V_{o,H}$ (voltage across an aHC at which its open probability, $P_{o,H}$, is 0.5) and A_H (coefficient characterizing the steepness of $P_{o,H}$ changes as a function of V_H). In addition, the S4SM allows us to define the actual number of Cx45 GJ channels with unitary conductance (γ_o) of 32 pS and residual conductance of ∼4 pS (24) that should be functional at any given time to explain the observed g_j (Fig. S2); N_F is the number of GJ channels with both slow gates open and with their fast V_j-gates open or closed, depending on pH_i and V_j. Thus, during the fitting process, $V_{o,H}$, A_H, and N_F were free parameters. The residual conductance and its rectification factor were additional free parameters.

Fitting of experimental g_j–V_j plots (gray lines in Figs. 2*B* and 3*B*) was performed assuming that each experimental g_j–V_j relation (black lines in Figs. 2*B* and 3*B*) is symmetric around V_j = 0 (Table S1 shows the parameters obtained to fit curves in Figs. 2*B* and 3*B*). In the S4SM we assumed the single aHC conductance ($\gamma_{o,H}$) for Cx45 was 64 pS (24) and that the residual conductance (γ_{res}) rectified so as to increase exponentially when the cytoplasmic side of the Cx45 aHC was more negative (legend in Fig. S1) (15).

The uncoupling effect of acidification with 5% CO_2 decreased $V_{o,H}$ by ∼35 mV and decreased g_j and N_F to near zero, whereas A_H remained virtually constant (Fig. 2*C* and Table S1). In contrast, alkalinization increased g_j 1.8-fold (Fig. 3*B*) and increased $V_{o,H}$ by ∼40 mV (Fig. 3*C*); there was a small increase in N_F, and A_H remained virtually constant (Table S1). The same effects on V_j gating were found in all seven experiments using intracellular acidification and all six experiments using alkalinization, including the one shown in Fig. S3, where both CO_2 and NH_4Cl were applied in the same experiment.

V_j dependence of the probabilities (P_S) of the four possible channel states [open-open (O-O), both aHCs open; open-closed

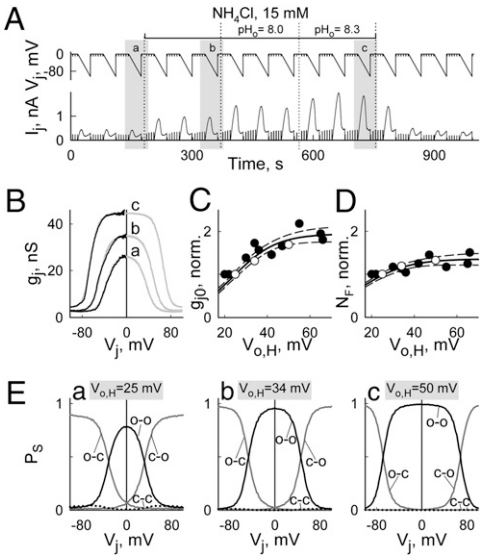

Fig. 3. V_j gating during alkalinization of homotypic Cx45 GJs. (*A*) I_j measured in a HeLaCx45 cell pair in response to repeated V_j ramps (31 s duration) from 0 to −100 mV before and during exposure to NH_4Cl alone or to NH_4Cl combined with alkaline conditions (pH_o = 8 or 8.3). V_j steps of −10 mV were used to measure g_j between V_j ramps. (*B*) Experimental g_j–V_j plots (in black) obtained at V_j ramps marked with gray rectangles in *A* were fitted to the S4SM (in gray) assuming that V_j gating was symmetric around V_j = 0. (*C*) Relation between g_j at V_j = 0 (g_{j0}; normalized to control/initial conditions) and $V_{o,H}$ (black and white circles). (*D*) Relation between N_F normalized to control/initial conditions and $V_{o,H}$ (black and white circles). Solid lines in *C* and *D* are fits to combined data from Fig. 2 and Fig. 3, obtained using a sigmoidal equation, $y = a/(1+e^{-(x-xo)/b})$ (n = 12). Dashed lines show 95% CI. White circles are from the experiment shown in *A*. (*E*) Probabilities of channels to dwell in O-O, C-O, O-C, and C-C states (P_S) depending on V_j and calculated for the three I_j records obtained at V_j ramps *a*–*c* marked with gray rectangles in *A*; calculated values of $V_{o,H}$ are indicated on each graph.

(O-C) and closed-open (C-O), one aHC open and one closed; and closed-closed (C-C), both aHCs closed (Fig. S2)] calculated with S4SM at acid, alkaline, and control pH_i is shown in Figs. 2*E* *a*–*c* and 3*E* *a*–*c*. The decrease in g_j during acidification was the result of a reduction of both $P_{O\text{-}O}$ (Figs. 2*E* *a*–*c*), caused by decrease in $V_{o,H}$ (Fig. 2*C*) and N_F (Fig. 2*D*). In contrast, increase in g_j during alkalinization was mainly the result of an increase of $P_{O\text{-}O}$ to ∼1 (Fig. 3*Ec*), caused by increase in $V_{o,H}$ (Fig. 3*C*), and a slight increase in N_F (Fig. 3*D*).

pH_i-Dependent Modulation of g_j and V_j Gating in Cx45/Cx43-EGFP Heterotypic GJ Channels. We examined the g_j–pH_i dependence of heterotypic Cx45/Cx43-EGFP GJs to study pH_i sensitivity of Cx45 aHCs and to test the hypothesis that pH_i sensitivity of aHCs is similar in homotypic and heterotypic GJs. Cx45 GJs are more sensitive to pH_i and V_j than Cx43-EGFP GJs, and the $P_{o,H}$ of the less sensitive Cx43-EGFP aHC changed relatively little over the pH_i and V_j range that changed the $P_{o,Cx45}$ aHC from high to low. For this reason we could evaluate the pH_i and V_j dependence of Cx45 aHCs at higher resolution in heterotypic than in homotypic junctions.

Homotypic Cx43 GJs show a pK_a between 6.6 and 6.7 (9, 25). We found that the pK_a of Cx43-EGFP GJs was slightly more acidic (pK_a = 6.50 ± 0.03, Hill coefficient **n** = 1.98, n = 6) (Fig. S4). Thus, the pK_a of Cx43-EGFP is ∼0.5 units more acidic than that of Cx45 (pK_a≈7) (Fig. 1). Cell pairs forming heterotypic Cx45/Cx43-EGFP GJs were selected based on EGFP expression in only one cell and the presence of one or more JPs between the cells (Fig. 4*A*). Junctional conductance (g_j) was measured by repeated application of V_j ramps from +10 to −10 mV and 600 ms in duration. Under control conditions (pH_i = 7.2), g_j varied between 15 and 71 nS (n = 18). To study pH_i effects on g_j, we perfused cells with MKR solution bubbled with different percentages of CO_2 or containing different concentrations of NH_4Cl (Fig. 4*B*). NH_4Cl increased g_j, which reached a plateau when exposed to MKR solutions with pH_o = 8.3 and containing 15 mM of NH_4Cl that increased pH_i to 8.3 ± 0.1 (n = 6). Here and below, we used alkaline MKR to increase pH_i; at neutral pH_o we would have needed 30 mM or more NH_4Cl to reach pH_i= 8.3, which might have been an excessive increase in osmolarity. The best fit of g_j–pH_i dependence by the Hill equation was obtained with pK_a = 6.70 ± 0.03 and Hill coefficient **n** = 1.6 (n = 6) (Fig. 4*C*). Hypothetically, the g_j–pH_i dependence of GJs results from the pH_i sensitivities of the two aHCs in series, and $P_o = P_{o,H1} \cdot P_{o,H2}$ (20). We estimated the $P_{o,H}$–pH_i dependence for Cx45 and Cx43-EGFP aHCs (Fig. 4*D*, dashed lines) by calculating the square root of P_o at each pH_i for homotypic GJs shown in Fig. 1*B* and Fig. S4, respectively. The P_o–pH_i relation and pK_a for heterotypic Cx45/C43-EGFP GJs falls between the P_o–pH_i relations and pK_as of the homotypic Cx45 and Cx43-EGFP GJs ($pK_{a,Cx45}$ ≈7; $pK_{a,Cx45/Cx43\text{-}EGFP}$ ≈ 6.7; $pK_{a,Cx43\text{-}EGFP}$ ≈ 6.5). Thus, to a first approximation, the product of $P_{o,H}$–pH_i dependence of Cx45 and Cx43-EGFP aHCs predicts the P_o–pH_i dependence of heterotypic GJs (Fig. 4*E*), suggesting that the series aHCs in heterotypic GJs respond independently to pH_i.

To examine pH_i effects on voltage-gating properties of Cx45/Cx43-EGFP GJs, we determined g_j–V_j relations at different pH_i by applying slow V_j ramps from 0 to +100 and −100 mV at the times indicated by the numbers on the g_j trace in Fig. 4*B*. In accordance with earlier reports (24, 26), the g_j–V_j dependence at pH_i = 7.2 was highly asymmetric around V_j = 0 (Figs. 4*F* and 5*B*). Both Cx45 and Cx43-EGFP aHCs exhibit negative gating polarity, i.e., they close at relative negativity on their cytoplasmic side (24). V_js for which the Cx45 side is relatively negative (which we define as positive V_j for Cx45/Cx43 heterotypic junctions) tend to close the Cx45 aHCs and open the Cx43 aHCs (Figs. 4*F* and 5*B*; gray lines are curves obtained with parameters shown in Table S2) (17). V_js of the opposite sign tend to close the Cx43-EGFP aHCs and open the Cx45 aHCs. In addition, Cx43-EGFP lacks the fast-gating mechanism and is significantly less V_j sensitive than Cx45 (27). Finally, in heterotypic Cx45/Cx43-EGFP channels with both aHCs open, a larger fraction of an applied V_j acts on the Cx45 aHC, because its conductance is ∼one-fourth that of the Cx43 aHC (24), and consequently Cx45 aHCs are more V_j sensitive in Cx45/Cx43-EGFP GJs than in Cx45/Cx45 GJs (22). As a result of these factors, V_j gating in Cx45/Cx43-EGFP GJs is determined mainly by the Cx45 aHCs at positive V_js, and the rightward shift of V_j sensitivity without change in slope along the V_j axis of heterotypic GJs during alkalinization (evident from data shown in Fig. 4*F*) is ascribable almost entirely to modulation of the Cx45 aHCs. Hence, Cx45 aHCs in homotypic GJs and heterotypic GJs with Cx43-EGFP exhibit similar modulation of V_j gating by pH_i. Figs. 4*G* and 5*C* show probabilities of the channels being in the O-O state during alkalinization and acidification, respectively, at times corresponding to those indicated in Figs. 4*F* and 5*B*. $P_{O\text{-}O}$–V_j plots show that alkalinization enhances $P_{O\text{-}O}$ over the entire V_j range, accounting for the rightward shift of the g_j–V_j relation (Fig. 4*F*), whereas acidification reduces $P_{O\text{-}O}$ and N_F, and shifts the $P_{O\text{-}O}$–V_j relation to the left, explaining the decrease in $P_{O\text{-}O}$ and g_j. At acid pH_i and V_j < −30 mV, $P_{O\text{-}O}$ decreases, presumably because of the Cx43 aHC closing. Figs. 4*H* and 5*D* show relations between g_{j0} (normalized to g_j at V_j = 0 and pH_i ≈ 7.2) and $V_{o,Cx45}$. Figs. 4*I* and 5*E* show relations between N_F (normalized to its value at pH_i ≈ 7.2) and $V_{o,Cx45}$. These relations were obtained from fits of g_j–V_j plots shown in Figs. 4*F* and 5*B*, respectively, and support

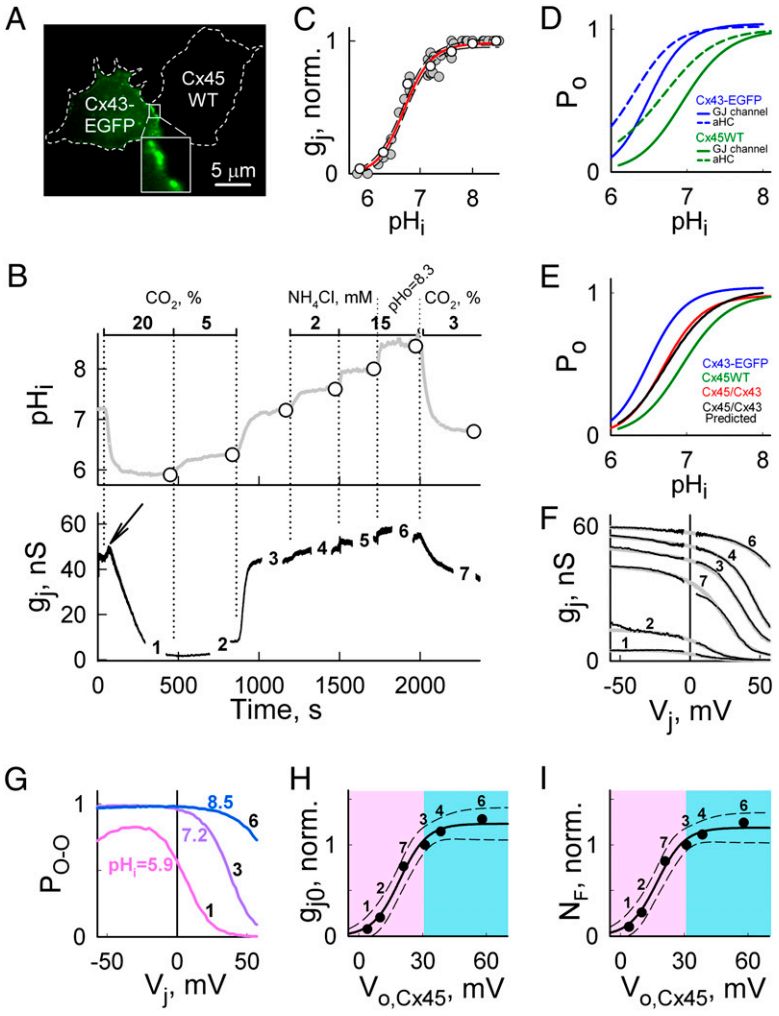

Fig. 4. pH_i-dependent modulation of g_j in heterotypic Cx45/Cx43-EGFP GJs. (*A*) Fluorescence image of a HeLa cell pair forming heterotypic Cx45/Cx43-EGFP GJs are enlarged in *Inset*. (*B*) pH_i and g_j measured in a Cx45/Cx43-EGFP cell pair exposed to CO_2 at the indicated percentages and at increasing concentrations of NH_4Cl alone or combined with alkaline MKR solution (pH_o = 8.3) and finally with 3% CO_2. (*C*) Junctional conductance (g_j)–pH_i dependence of Cx45/Cx43-EGFP GJs (white circles are from the experiment shown in *B* and gray circles are from other five experiments). The red line shows fit of the Hill equation to the data; pK_a = 6.70 ± 0.03, Hill coefficient **n** = 1.6 (n = 6). Dashed lines show 95% CI. (*D*) P_o–pH_i dependence of Cx45 (green) and Cx43-EGFP (blue) homotypic GJs calculated from data shown Fig. 1 and Fig. S4, respectively. Dashed green and blue lines are square roots of P_o–pH_i dependence of Cx45 and Cx43-EGFP homotypic GJs, respectively. (*E*) P_o–pH_i dependence of Cx45 (green), Cx43-EGFP (blue), and Cx45/Cx43-EGFP (red) GJs. The black line shows the product of $P_{o,Cx45}$–pH_i and $P_{o,Cx43}$–pH_i plots shown in *D* (predicted). (*F*) Junctional conductance (g_j)–V_j plots (black lines) calculated by applying pairs of V_j ramps (35 s duration) from 0 to +100 and to −100 mV at the numbered times shown on the g_j trace in *B*. Gray lines show calculated g_j–V_j plots fit by the S4SM to the experimental data. (*G*) Probabilities of channels being in the O-O state at times of ramps #1, #3, and #6 obtained from fits to g_j–V_j plots with indicated pH_is and numbers corresponding to those shown in *F*. (*H*) Relation between g_j normalized to g_j at V_j = 0 under control conditions (g_{j0}, norm.) and $V_{o,\ Cx45}$. (*I*) Relation between N_F normalized to N_F at pH = 7.2 and $V_{o,Cx45}$. Acidic conditions are shown in light pink, and alkaline conditions are shown in light blue relative to pH_i = 7.2. Solid lines in *H* and *I* are fits of a sigmoidal equation, $y = a/(1+e^{-(x-xo)/b})$. Dashed lines show 95% CI.

the conclusion reached in Cx45 homotypic GJs that acidification decreases g_j because of the decrease in $V_{o,H}$ and N_F.

Functional Efficiency of Cx45-EGFP GJ Channels. We have reported that only ∼1/10 of Cx43-EGFP and ∼1/100 of Cx57 channels assembled into JPs are open at any one time at V_j = 0, and we called this fraction (K) "functional efficiency" (19, 28). To estimate K for Cx45-EGFP GJs, we used the same approach. In brief, we selected cell pairs with JPs that were oriented parallel to the focal plane and could be viewed *en face* (Fig. 6*A*). To obtain fluorescence per unit area without edge effects, we selected JPs that were sufficiently large so that the fluorescence was uniform in a central region. We assessed fluorescence per unit area (F_{JP}) in this region in arbitrary fluorescent units (a.u.) and subtracted background fluorescence outside the JP. We assumed that each Cx45-EGFP channel occupied 100 nm^2 (corresponding to 10-nm center-to-center spacing in a square array and 10^4 channels per μm^2) as an approximation of values seen in atomic force microscopy (29, 30). Thus, we assessed the fluorescence produced by a single GJ channel (F_γ) from the ratio F_{JP}/10,000; on average F_γ = 0.173 ± 0.001 a.u. (n = 19).

In combined imaging and electrophysiological studies, we measured g_j and the total fluorescence intensity (F_T) of JPs independent of their spatial orientation. F_T was estimated by measuring the total fluorescence in the region of interest (ROI) enclosing a JP (dashed ellipse in Fig. 6*B*). To collect all light including that from regions that were not in the exact focus, the ROI was made several fold larger than the size of the JPs (28). The total number of GJ channels present in each JP (N_T) was determined from the ratio, $N_T = F_T/F_\gamma$. JPs with ∼4.6×10^3 to 75×10^3 GJ channels (n = 14) based on fluorescence ranged from ∼1–4 µm in diameter. During exposure to MKR solution at pH_o = 8.3 and containing 10 mM NH_4Cl, $P_{O\text{-}O}$ at V_j = 0 was equal to 0.98 ± 0.03 (n = 6) (Fig. 3*Ec* and Fig. S3*Ec*), and N_F approached a maximum, N_{Fmax}, which is equal to maximum g_j (g_{jmax})/γ_o. We hypothesize that $P_{O\text{-}O}$ for these channels was ∼1 and that $P_{O\text{-}O}$ for the remaining, nonfunctional channels was ∼0. Thus, the fraction of functional channels is the ratio of N_{Fmax} to the total number of channels, $K = N_{Fmax}/N_T$. We found that under alkaline conditions for GJs ranging from 102 to 3,160 channels, N_{Fmax} was linearly related to N_T with K = 0.039 ± 0.003 (n = 14) (Fig. 6*C*), and the fraction of functional channels is ∼1/25.

Discussion

Here we propose that an increase of g_j between Cx45-expressing cells with alkalinization from normal pH_i is caused mainly by an increase in open probability, $P_{O\text{-}O}$, of the functional channels. Acidification-induced full uncoupling is approached by decrease in both $P_{O\text{-}O}$ and N_F. The parameter A_H characterizing steepness of g_j dependence on V_H, remained virtually constant during pH_i changes, suggesting that the gating charge involved in voltage sensing did not change significantly. Generally, g_j–V_j dependence has been used to compare and characterize GJ channels formed by different Cx isoforms (31). Here we demonstrated that V_j

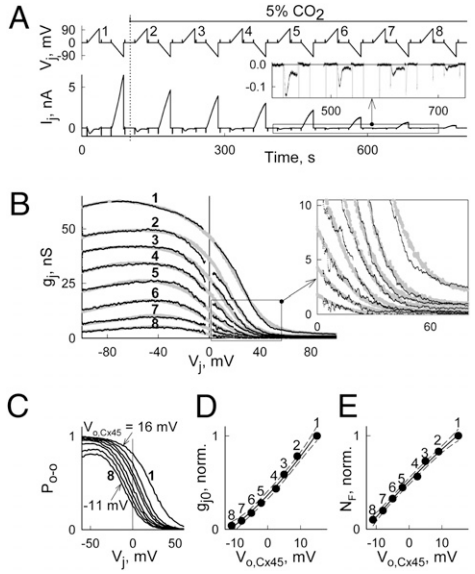

Fig. 5. V_j gating during acidification of heterotypic Cx45/Cx43-EGFP GJs. (*A*) I_j measured in a Cx45/Cx43-EGFP cell pair in response to repeated V_j ramps (25 s duration) from 0 to −100 mV and to +100 mV, and short (500-ms) steps of 20 mV during application of 5% CO_2. (*B*) Junctional conductance (g_j)–V_j data (black lines), calculated from V_j and I_j records marked with numbers from 1 to 8 shown in *A*, were fit by the S4SM (in gray). (*C*) Probability that GJs dwell in the O-O state as a function of V_j; attached numbers correspond to those shown in *A* and *B*. (*D*) Relation between g_j normalized to its value under control conditions at V_j = 0 (g_{j0}, norm.) and $V_{o,Cx45}$; numbers correspond to those shown in *A* and *B*. (*E*) Relation between N_F normalized to N_F at pH = 7.2 and $V_{o,Cx45}$. Solid lines in *D* and *E* are fit to the data using a linear regression of the second order. Dashed lines show 95% CI.

gating can be modulated by pH_i (see also ref. 32). For example, Cx45 GJs, which are highly V_j sensitive at normal pH_i, can be modulated by intracellular alkalinization, so that their g_j–V_j dependence resembles that of connexin26, which is relatively V_j insensitive around V_j = 0. Similar changes were reported for connexin 57 (Cx57) (19). Fluorescence imaging showed that the size of Cx45-EGFP and Cx43-EGFP homotypic GJs remained constant during exposure to and recovery from CO_2 or NH_4Cl (for Cx43-EGFP, see ref. 27). Furthermore, the pH_i-dependent changes in g_j over the time intervals measured appeared too fast and reversible to result from de novo formation or internalization of GJ channels. Fitting analysis showed that with increasing alkalinization P_{O-O} increases asymptotically to a maximum that we hypothesize is unity at V_j = 0. If so, only ~1/25 of Cx45-EGFP channels assembled into JPs are functional, i.e., can be activated by changes in V_j and pH_i (Fig. 6). The presence of such a small fraction of functional channels is not unique to Cx45 but also applies to Cx43 (28) and Cx57 (19), and their functionality may be determined by factors such as time needed for maturation after docking of two hemichannels, interaction with other proteins, and phosphorylation, which may move channels between functional and nonfunctional populations. Moreover, channels not mediating cell–cell coupling may be involved in other functions.

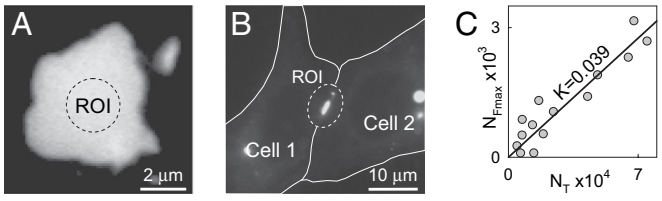

Fig. 6. Functional efficiency of HeLaCx45-EGFP GJs. (*A*) Fluorescence image of a region where two cells overlap and form a JP oriented parallel to the focal plane. The area encircled by the dashed line is the region of interest (ROI) in which fluorescence intensity could be measured without edge effects because of the large size of the JP. (*B*) Image of a HeLaCx45 cell pair forming a JP enclosed in an ROI. Solid lines indicate cell borders. (*C*) The relation between N_{Fmax} estimated from g_j measurements and N_T. Linear regression (solid line) shows that under alkaline conditions N_{Fmax} was linearly related to N_T with slope of 0.039 ± 0.03. Thus, only ~4% of GJ channels are functional.

We found that pK_a of Cx45/Cx43-EGFP heterotypic GJs is equal to 6.7, which is between pK_as measured for GJs formed by Cx45 (Fig. 1*B*; $pK_a \approx 7.0$) and Cx43-EGFP (Fig. S4*B*; $pK_a \approx 6.5$). pK_a reported for wild-type Cx43 measured in *Xenopus* oocytes (9) and Novikoff hepatoma cells (21) is 6.7; thus, attachment of EGFP to Cx43 C terminus appears to acidify $pK_{a,Cx43\text{-}EGFP}$ by ~0.2 units as well as to eliminate the fast-gating mechanism (27). In the pH_i range of 6.7–8.0, Cx45 aHCs largely determine g_j of Cx45/Cx43-EGFP heterotypic GJs. Theoretically, if the two aHCs in series act independently, the g_j–pH_i dependence of GJs results from pH_i sensitivities of both aHCs in series, and pK_a should be ~6.7, as observed experimentally (Fig. 4*E*). Thus, in these heterotypic junctions, at least, docking of unapposed hemichannels appears not to affect their sensitivity to pH_i.

Similarly, V_j gating in Cx45/Cx43-EGFP GJs should be determined mainly by the Cx45 aHC for two reasons: (*i*) Cx45 is more V_j sensitive than Cx43-EGFP in homotypic junctions (24), and (*ii*) most of the V_j drops across the Cx45 aHC because of its ~3.6-fold lower conductance, resulting in an increase and decrease of V_j gating of Cx45 and Cx43-EGFP aHCs, respectively (22). In Cx45/Cx43-EGFP heterotypic GJs, sensitivity to V_j around V_j = 0 is caused mainly by changes in the Cx45 aHC.

Changes in pH_i have important effects on cell function. For example, in cardiac muscle changes in pH_i influence normal tissue function by affecting excitability, contractility, and intercellular communication through GJs (33). This pH-dependent modulation of GJ channels may be critical under severe pathological conditions, because the uncoupling effect of low pH_i may reduce propagation of metabolic stress from damaged cells to healthy neighbors (34, 35) or prevent rescue of stressed cells by healthier neighbors, as discussed later. Brief periods of global ischemia can produce fast intracellular acidosis of ~0.4 pH units in isolated ferret hearts (36). Increase in impulse frequency rate from 1 to 3 Hz causes a decrease in pH_i by ~0.3 units in isolated sheep Purkinje fibers (37). pH_i decreases more dramatically during global ischemia in a perfused rat heart model (38) when pH_i drops to ~6.2, which accounts for much of the observed failure of contraction (36). A pH_i decrease from 7.2 to 6.8 in cells expressing Cx45 would reduce g_j more than twofold. This change would affect cell–cell metabolic communication, electrical signaling, and, consequently, the conduction of excitation in tissues where Cx45 is expressed extensively, e.g., the conduction system of the heart (39), smooth muscle cells of blood vessels (40), and certain neurons (41). Furthermore, Cx45 knock-out mice die in utero because of atrioventricular conduction block, impairment of atrial contraction, and severe dilation of the heart (42, 43).

Ischemia can result in local acidosis where capillary perfusion is greatly reduced, and neighboring less acid-loaded regions can help maintain pH by diffusion of hydrogen ions through the extracellular and intracellular compartments. Connexin-based GJ channels and hemichannels may serve as conduits for intracellular acid dissipation, especially because the classical sarcolemmal routes for acid efflux appear to be inhibited (44). Studies of normal/ischemia border regions in isolated preparations of the heart showed that preservation of ischemic cells by neighboring cells exposed to normal perfusion is greater in the longitudinal than in transverse direction of the fibers, consistent with ~7- to 10-fold stronger cell–cell coupling in the longitudinal direction (45). However, under severe ischemic conditions GJ communication is blocked (46), and this blockage may limit both the spread of damage and the cell-rescuing/

preservation effect of GJs. Thus, during mild ischemia GJs remain open to preserve ischemia-affected cells, but when ischemia worsens, GJs shut down, a response that may isolate damaged areas and improve organ survival.

In summary, modulation at alkaline pH of cell–cell coupling of Cx45 homotypic and Cx45/Cx43 heterotypic GJ channels can be explained largely by changes in $V_{o,H}$ with little change in A_H and N_F. Acidification decreases the number of functional channels and shifts $V_{o,H}$ so as to reduce $P_{O\text{-}O}$, while A_H remains constant. The decrease in $V_{o,H}$ appears continuous over the entire pH range investigated. i.e., ~6–8, suggesting a single mechanism. Cx45 GJ channels contain both fast and slow gates. Although we cannot yet clearly separate the effects of fast and slow gates on V_j- and pH_i-dependent gating, we hypothesize that pH_i affects N_F through modulation of the slow gate, whereas changes in V_j gating are largely determined by the fast gate.

Methods

SI Text includes details of the experimental procedures.

Experiments with homotypic junctions were performed on HeLa cells transfected with wild-type Cx45, Cx45-EGFP, or Cx43-EGFP. Experiments with heterotypic junctions were performed on cocultures of HeLa cells expressing Cx45 or Cx43-EGFP. Junctional conductance (g_j) was measured using the dual whole-cell voltage clamp method (15). Fluorescence signals were acquired using UltraVIEW software for image acquisition and analysis (Perkin-Elmer Life Sciences). For ratiometric pH_i measurement, the unesterified form of BCECF (10 μM) was introduced into the cells through patch pipettes in whole-cell voltage-clamp mode. Dye was excited alternately with low-intensity 436-nm and 500-nm light for 0.5 s every 15 s (to minimize photobleaching), and the emitted light was filtered at 540 nm.

ACKNOWLEDGMENTS. We thank Angele Bukauskiene for excellent technical assistance. This work was supported by National Institutes of Health Grants NS036706 and HL084464 to F.F.B. and NS045287 to M.V.L.B.

1. Demaurex N (2002) pH Homeostasis of cellular organelles. *News Physiol Sci* 17:1–5.
2. Delmar M, Coombs W, Sorgen P, Duffy HS, Taffet SM (2004) Structural bases for the chemical regulation of connexin43 channels. *Cardiovasc Res* 62:268–275.
3. Sáez JC, Retamal MA, Basilio D, Bukauskas FF, Bennett MVL (2005) Connexin-based gap junction hemichannels: Gating mechanisms. *Biochim Biophys Acta* 1711:215–224.
4. Obara M, Szeliga M, Albrecht J (2008) Regulation of pH in the mammalian central nervous system under normal and pathological conditions: Facts and hypotheses. *Neurochem Int* 52:905–919.
5. Chesler M, Kaila K (1992) Modulation of pH by neuronal activity. *Trends Neurosci* 15: 396–402.
6. Lyall V, Biber TU (1994) Potential-induced changes in intracellular pH. *Am J Physiol* 266:685–696.
7. Diarra A, Sheldon C, Brett CL, Baimbridge KG, Church J (1999) Anoxia-evoked intracellular pH and Ca2+ concentration changes in cultured postnatal rat hippocampal neurons. *Neuroscience* 93:1003–1016.
8. Madden JA, Keller PA, Kleinman JG (2000) Changes in smooth muscle cell pH during hypoxic pulmonary vasoconstriction: A possible role for ion transporters. *Physiol Res* 49:561–566.
9. Stergiopoulos K, et al. (1999) Hetero-domain interactions as a mechanism for the regulation of connexin channels. *Circ Res* 84:1144–1155.
10. Trexler EB, Bukauskas FF, Bennett MVL, Bargiello TA, Verselis VK (1999) Rapid and direct effects of pH on connexins revealed by the connexin46 hemichannel preparation. *J Gen Physiol* 113:721–742.
11. Peracchia C (2004) Chemical gating of gap junction channels; roles of calcium, pH and calmodulin. *Biochim Biophys Acta* 1662:61–80.
12. Hirst-Jensen BJ, Sahoo P, Kieken F, Delmar M, Sorgen PL (2007) Characterization of the pH-dependent interaction between the gap junction protein connexin43 carboxyl terminus and cytoplasmic loop domains. *J Biol Chem* 282:5801–5813.
13. Duffy HS, et al. (2004) Regulation of connexin43 protein complexes by intracellular acidification. *Circ Res* 94:215–222.
14. Barker RJ, Price RL, Gourdie RG (2002) Increased association of ZO-1 with connexin43 during remodeling of cardiac gap junctions. *Circ Res* 90:317–324.
15. Rackauskas M, et al. (2007) Gating properties of heterotypic gap junction channels formed of connexins 40, 43, and 45. *Biophys J* 92:1952–1965.
16. Palacios-Prado N, Bukauskas FF (2009) Heterotypic gap junction channels as voltage-sensitive valves for intercellular signaling. *Proc Natl Acad Sci USA* 106:14855–14860.
17. Bukauskas FF, Verselis VK (2004) Gap junction channel gating. *Biochim Biophys Acta* 1662:42–60.
18. Harris AL (2001) Emerging issues of connexin channels: Biophysics fills the gap. *Q Rev Biophys* 34:325–472.
19. Palacios-Prado N, Sonntag S, Skeberdis VA, Willecke K, Bukauskas FF (2009) Gating, permselectivity and pH-dependent modulation of channels formed by connexin57, a major connexin of horizontal cells in the mouse retina. *J Physiol* 587:3251–3269.
20. Spray DC, Harris AL, Bennett MVL (1981) Gap junctional conductance is a simple and sensitive function of intracellular pH. *Science* 211:712–715.
21. Lazrak A, Peracchia C (1993) Gap junction gating sensitivity to physiological internal calcium regardless of pH in Novikoff hepatoma cells. *Biophys J* 65:2002–2012.
22. Paulauskas N, Pranevicius M, Pranevicius H, Bukauskas FF (2009) A stochastic four-state model of contingent gating of gap junction channels containing two "fast" gates sensitive to transjunctional voltage. *Biophys J* 96:3936–3948.
23. Harris AL, Spray DC, Bennett MVL (1981) Kinetic properties of a voltage-dependent junctional conductance. *J Gen Physiol* 77:95–117.
24. Bukauskas FF, Angele AB, Verselis VK, Bennett MVL (2002) Coupling asymmetry of heterotypic connexin 45/ connexin 43-EGFP gap junctions: Properties of fast and slow gating mechanisms. *Proc Natl Acad Sci USA* 99:7113–7118.
25. Morley GE, Taffet SM, Delmar M (1996) Intramolecular interactions mediate pH regulation of connexin43 channels. *Biophys J* 70:1294–1302.
26. Moreno AP, Fishman GI, Beyer EC, Spray DC (1995) Voltage dependent gating and single channel analysis of heterotypic gap junction channels formed of Cx45 and Cx43. *Intercellular Communication Through Gap Junctions, Progress in Cell Research.*, eds Kanno Y, et al. (Elsevier Science B.V., Amsterdam), Vol 4, pp 405–408.
27. Bukauskas FF, Bukauskiene A, Bennett MVL, Verselis VK (2001) Gating properties of gap junction channels assembled from connexin43 and connexin43 fused with green fluorescent protein. *Biophys J* 81:137–152.
28. Bukauskas FF, et al. (2000) Clustering of connexin 43-enhanced green fluorescent protein gap junction channels and functional coupling in living cells. *Proc Natl Acad Sci USA* 97:2556–2561.
29. Müller DJ, Hand GM, Engel A, Sosinsky GE (2002) Conformational changes in surface structures of isolated connexin 26 gap junctions. *EMBO J* 21:3598–3607.
30. Lal R, John SA, Laird DW, Arnsdorf MF (1995) Heart gap junction preparations reveal hemiplaques by atomic force microscopy. *Am J Physiol* 268:C968–C977.
31. González D, Gómez-Hernández JM, Barrio LC (2007) Molecular basis of voltage dependence of connexin channels: An integrative appraisal. *Prog Biophys Mol Biol* 94: 66–106.
32. Bennett MVL, Verselis V, White RL, Spray DC (1988) Gap junctional conductance: Gating. *Gap Junctions*, eds Hertzberg EL, Johnson RG (Alan R. Liss,Inc., New York), pp 287–304.
33. Komukai K, Brette F, Orchard CH (2002) Electrophysiological response of rat atrial myocytes to acidosis. *Am J Physiol Heart Circ Physiol* 283:H715–H724.
34. Délèze J (1970) The recovery of resting potential and input resistance in sheep heart injured by knife or laser. *J Physiol* 208:547–562.
35. Bukauskas F (1982) Electrophysiology of the normal-to-hypoxic transition zone. *Circ Res* 51:321–329.
36. Elliott AC, Smith GL, Eisner DA, Allen DG (1992) Metabolic changes during ischaemia and their role in contractile failure in isolated ferret hearts. *J Physiol* 454:467–490.
37. Bountra C, Kaila K, Vaughan-Jones RD (1988) Mechanism of rate-dependent pH changes in the sheep cardiac Purkinje fibre. *J Physiol* 406:483–501.
38. Garlick PB, Radda GK, Seeley PJ (1979) Studies of acidosis in the ischaemic heart by phosphorus nuclear magnetic resonance. *Biochem J* 184:547–554.
39. Kreuzberg M, et al. (2006) Connexin 30.2 containing gap junction channels decelerate impulse propagation through the atrioventricular node. *Proc Natl Acad Sci USA* 108: 5959–5964.
40. Li X, Simard JM (2001) Connexin45 gap junction channels in rat cerebral vascular smooth muscle cells. *Am J Physiol Heart Circ Physiol* 281:H1890–H1898.
41. Veruki ML, Hartveit E (2009) Meclofenamic acid blocks electrical synapses of retinal AII amacrine and on-cone bipolar cells. *J Neurophysiol* 101:2339–2347.
42. Krüger O, et al. (2000) Defective vascular development in connexin 45-deficient mice. *Development* 127:4179–4193.
43. Kumai M, et al. (2000) Loss of connexin45 causes a cushion defect in early cardiogenesis. *Development* 127:3501–3512.
44. Allen DG, Xiao XH (2003) Role of the cardiac Na+/H+ exchanger during ischemia and reperfusion. *Cardiovasc Res* 57:934–941.
45. Bukauskas FF, Gutman AM, Kisunas KJ, Veteikis RP (1982) Electrical cell coupling in rabbit sino atrial node and atrium. Experimental and theoretical evaluation. *Cardiac Rate and Rhythm. Physiological, Morphological and Developmental Aspects*, eds Bouman LN, Jongsma HJ (Martinus Nijhoff Publishers, The Hague), pp 195–216.
46. Wojtczak J (1979) Contractures and increase in internal longitudinal resistance of cow ventricular muscle induced by hypoxia. *Circ Res* 44:88–95.